Chemical Engineering Journal 414 (2021) 128838

Contents lists available at ScienceDirect

Chemical Engineering Journal

journal homepage: www.elsevier.com/locate/cej

Impact of toluene poisoning on MnCe/HZSM-5 SCR catalyst

Peng Lu [a,b], Lyumeng Ye [c], Xianhui Yan [a,b], Ping Fang [a,b], Xiongbo Chen [a,b], Dingsheng Chen [a,b], Chaoping Cen [a,b,*]

[a] Guangdong Province Engineering Laboratory for Air Pollution Control, South China Institute of Environmental Sciences, MEE, Guangzhou 510655, PR China
[b] Guangdong Provincial Key Laboratory of Water and Air Pollution Control, Guangzhou 510655, PR China
[c] School of Environmental Science and Engineering, Sun Yat-sen University, Guangzhou 510275, PR China

ARTICLE INFO

Keywords:
MnCe/HZSM-5
NH_3-SCR
Toluene catalytic oxidation
Simultaneous removal
Lewis acid sites

ABSTRACT

Increasing attentions have been drawn towards the simultaneous removal of toluene in current existing NH_3-SCR unit. The development of dual-functional catalysts and the understanding of impact induced by toluene addition are momentous but lacking. Herein, a well-reported MnO_x-CeO_2 catalyst was chosen as active phase to assess the role of HZSM-5 in this simultaneous removal process. HZSM-5 was found to supply more acid sites especially Lewis acid on the MnO_x-CeO_2 catalyst. A MnCe/HZSM-5 catalyst with a SiO_2/Al_2O_3 molar ratio of 25 delivered a broad active temperature window of 200–400 °C with NO conversion > 80% and possessed a stable N_2 selectivity > 96% in NH_3-SCR reaction. Also, it was able to maintain above 60% of toluene conversion in the range of 200–400 °C. More Lewis acid sites, together with abundant Mn^{4+}, Ce^{3+} and active surface oxygen that formed via the interaction between Mn^{4+}/Mn^{3+} and Ce^{4+}/Ce^{3+} ($Mn^{3+} + Ce^{4+} \leftrightarrow Mn^{4+} + Ce^{3+}$), contributed to the superior catalytic performance of MnCe/HZSM-5 with lower SiO_2/Al_2O_3 ratio. A reversible catalyst deactivation in NH_3-SCR induced by toluene was found. Toluene was prone to reacting with NH_3 forming nitriles, which infringed the active sites and decreased the available coordinated NH_3 on Lewis acid sites. In addition, the suppression of NO oxidation to NO_2 that decreasing the percentage of "fast SCR" process, and the inhibition of NH_3 activation to NH_2 species also contributed to the lower SCR activity in the presence of toluene over MnCe/HZSM-5.

1. Introduction

As the precursors of tropospheric ozone and secondary organic aerosol, nitrogen oxides (NO_x) and volatile organic compounds (VOCs, such as toluene) are widely emitted from stationary sources, such as fossil fuel, biomass and solid wastes combustion, damaging the ecological environment and endangering the public [1]. Catalytic removal is considered to be one of the most potential methods for the complete reduction of NO_x and oxidation of toluene. Recent years, simultaneously catalytic abatement of NO_x and toluene has gained increasing attentions due to the similar redox property requirement of catalysts [2–4]. During this process, the NO_x is reduced to N_2, while the toluene is oxidized to CO_2 and H_2O. Considering the advantages of high feasibility and low cost, the co-removal of toluene in single NH_3-SCR unit is highly desirable, which demands rational designed dual-functional catalysts.

Currently, V-based catalysts (V_2O_5-$WO_3(MoO_3)/TiO_2$, VC, Ce-VC, V_2O_5/TiO_2-CNTs, etc.) [4–8], Mn-based catalysts (MnO_x-CeO_2, Fe/α-MnO_2, etc.) [1,3,9–11], and Ce-based catalysts ($CuCeAl_x$, $Ce_{0.2}TiAl_\alpha O_x$, etc.) [2,12], have been explored for the possibility of synergistic removal of NO_x and VOCs. Among these catalysts, MnO_x catalysts are very attractive because of excellent low-temperature activity resulted from variable valance states, high redox ability and oxygen storage capacity [13,14]. CeO_2 has been extensively investigated to promote the activity and stability of MnO_x catalysts. MnO_x-CeO_2 composites have shown superior catalytic performance in catalytic reactions as a consequence of the redox shift between Mn^{4+}/Mn^{3+} and Ce^{4+}/Ce^{3+} ($Mn^{3+} + Ce^{4+} \leftrightarrow Mn^{4+} + Ce^{3+}$), generating the interactions between Mn/Ce oxides, oxygen vacancy and active oxygen species with high mobility [15]. However, the MnO_x-CeO_2 catalysts still face the problems of narrow activity temperature window and poor N_2 selectivity. One effective strategy to solve these problems is the usage of support, which increases the MnO_x/CeO_2 dispersion and promotes the electron transfer within active components. The ZSM-5 zeolite (e.g., HZSM-5) has been

* Corresponding author at: South China Institute of Environmental Sciences, MEE, Guangzhou 510655, PR China.
E-mail address: cenchaoping@scies.org (C. Cen).

https://doi.org/10.1016/j.cej.2021.128838
Received 25 November 2020; Received in revised form 23 January 2021; Accepted 1 February 2021
Available online 7 February 2021

widely applied as a carrier in catalytic reactions owing to adjustable surface acidity, large surface area, shape selectivity and thermal/hydrothermal stability [16,17]. MnCe/ZSM-5 has been proved to be a good SCR catalyst with wide activity temperature window and N_2 selectivity, and a potential catalyst for toluene catalytic oxidation as well [15,16,18,19]. To date, to the best of the authors' knowledge there is no report studying the simultaneous removal of NO_x and toluene over MnCe/ZSM-5 catalysts.

The understanding of impact induced by VOCs addition on SCR performance is crucial for the catalyst design and technology application. Previous research mainly focused on the influence of toxic chlorobenzene (CB) and dioxins. More recently, the influence of toluene, one of the major precursors of ozone and $PM_{2.5}$, has been preliminarily studied. Zhao et al. [2] speculated that toluene could be the reducing agent of NO, which was beneficial to SCR reaction on Al_2O_3-modified CuO-CeO_2 catalyst. On the contrary, Ye at al. [1] observed the low-temperature SCR activity of MnO_x-CeO_2 catalyst was inhibited owing to the competitive adsorption of toluene, the decreasing of active Lewis acid sites, and the increasing of unfavored oxidation reactions of NH_3. The contradictory results in a very limited number of relevant literature show that the effects of toluene on NH_3-SCR performance (e.g., NO conversion, side reactions and N_2 selectivity) are still unclear, and the collaborative removal mechanism urgently needs further investigation.

In this work, MnCe/HZSM-5 catalysts for simultaneous removal of NO_x and toluene were prepared via impregnation method. MnCe/γ-Al_2O_3 was also synthesized for comparison purpose. Performance testing and systematic characterization (XRD, BET, XPS, Py-IR, TGA, NH_3-TPD and *in situ* DRIFTs) were conducted to investigate the SCR and toluene catalytic oxidation activities over MnCe/HZSM-5 catalysts with different SiO_2/Al_2O_3 molar ratios. Moreover, the impact of toluene addition on NH_3-SCR performance over MnCe/HZSM-5 was discussed.

2. Experimental

2.1. Catalyst synthesis

MnCe/HZSM-5 catalysts were synthesized by a conventional wet impregnation method. Certain amounts of $Mn(NO_3)_2$, $Ce(NO_3)_3{\cdot}6H_2O$ and HZSM-5 were mixed in ethanol and continuously stirred for 5 h, followed by drying at 105 °C for 12 h and calcined at 550 °C in air for 5 h. The molar ratio of Mn/Ce in catalysts was 1:1, whereas the mass ratio of HZSM-5 support was 80%. The prepared catalysts were denoted as MnCe/HZSM5-25, MnCe/HZSM5-100 and MnCe/HZSM5-360 according to the SiO_2/Al_2O_3 molar ratios (25, 100 and 360) of HZSM-5. For comparison purpose, MnCe/γ-Al_2O_3 was also synthesized following the same preparation route. HZSM-5 was purchased from Nankai University Catalyst Co., Ltd. (Tianjin, P. R. China). $Mn(NO_3)_2$, $Ce(NO_3)_3{\cdot}6H_2O$ and γ-Al_2O_3 were supplied by Shanghai Aladdin Bio-Chem Technology Co., Ltd. (Shanghai, P. R. China).

2.2. Catalyst characterization

A powder X-ray diffractometer equipped with Cu Kα radiation (model D/max RA, Rigaku Co., Japan) was applied to obtain the XRD patterns. The data were recorded in the 2θ range of 10–90° with a step size of 0.02°. N_2 adsorption–desorption isotherm was obtained by a chemisorption analyzer (Micromeritics ASAP 2020, USA). Specific surface area was calculated through Brunauer–Emmett–Teller (BET) method. Mn, Ce and O binding energies were examined by X-ray photoelectron spectroscopy (XPS, Thermo Scientific ESCALAB 250) with Al Kα X-ray radiation (1486.6 eV) operated at 150 W. Thermogravimetric analysis (TGA) was conducted on a DSC/DTA-TG (STA 449 F3 Jupiter, NETZSCH) to obtain the amount of the byproduct deposited on the used catalyst and record the reaction heat as well. ~8 mg samples were programmed to 850 °C with a rate of 10 °C/min in 100 mL/min air atmosphere. Detailed descriptions towards the pyridine adsorbed IR spectroscopy (Py-IR), the temperature programmed desorption (NH_3-TPD, $NH_3 + C_7H_8$-TPD, $NO + O_2$-TPD and $NO + O_2 + C_7H_8$-TPD) and the *in situ* diffuse reflectance infrared Fourier transform spectroscopy (DRIFTs) were illustrated in **Supporting Information**.

2.3. Catalytic activity measurement

The SCR and toluene catalytic oxidation activities were measured in a fixed-bed quartz tube reactor from 50 to 400 °C. The internal diameter of the quartz tube was 8 mm. The flow rate of feed gas was 200 mL/min, passing through 0.2 g catalyst, and the corresponding gas hourly space velocity (GHSV) was 60,000 mL/(g·h). The feed gas contained 500 ppm NH_3, 500 ppm NO, 10 vol% O_2, 50 ppm C_7H_8 (when used), and balance of N_2. The compositions of outlet gas (NH_3, NO, N_2O, NO_2, C_7H_8 and CO_2, etc.) were continuously monitored by an on-line FT-IR spectrometer (GASMET DX-4000, Finland).

The NO conversion (%), N_2 selectivity (%) in SCR reaction and toluene conversion (%) in catalytic oxidation reaction were calculated by **Eqs. (1)–(3)**. The kinetic analysis method was supplied in **Supporting information**.

$$NO\ conversion\ (\%) = \frac{C_{NO}^{in} - C_{NO}^{out}}{C_{NO}^{in}} \times 100\% \quad (1)$$

$$N_2\ selectivity\ (\%) = \left(1 - \frac{2C_{N_2O}^{out}}{C_{NO_x}^{in} + C_{NH_3}^{in} - C_{NO_x}^{out} - C_{NH_3}^{out}}\right) \times 100\% \quad (2)$$

$$Toluene\ conversion\ (\%) = \frac{C_{toluene}^{in} - C_{toluene}^{out}}{C_{toluene}^{in}} \times 100\% \quad (3)$$

3. Results and discussion

3.1. Catalyst characterization

As shown in **Fig. S1**, the differences of XRD patterns between MnCe/HZSM-5 catalysts were insignificant, and all catalysts yielded the characteristic peaks of HZSM-5 at 20–30°, 45.4° and 55.5°, suggesting that the loading of Mn and Ce oxides did not change the HZSM-5 structure [20]. The characteristic peaks of CeO_2 with a cubic fluorite structure (JCPDS: 34-0394) appeared at 2θ = 28.7° and 47.3°. The diffraction peaks at 2θ = 32.9° and 37.2° were attributed to the Mn_3O_4 (JCPDS: 18-0803).

The BET surface area and pore volume of MnCe/HZSM-5 were 208–305 m^2/g and 0.125–0.165 cm^3/g (**Table S1**), respectively, showing an increasing trend with a higher SiO_2/Al_2O_3 ratio. The surface area of HZSM-5 modified MnO_x-CeO_2 catalysts was massively larger than the MnO_x-CeO_2 catalysts of 71.6 m^2/g [1]. Relatively high surface area is beneficial for the dispersion of Mn/Ce oxides. According to the International Union of Pure and Applied Chemistry (IUPAC) classification, the N_2 adsorption–desorption isotherms of MnCe/HZSM-5 catalysts were typical type I isotherms (**Fig. S2**) [21]. The quantity of adsorbed gas rapidly increased at low relative pressure, which was associated with large amount of micropores that typically indicated strong adsorption potential. The appearance of adsorption hysteresis at high relative pressure indicated the co-existence of micro- and mesopores.

The pyridine-IR was conducted to evaluate the acidity of MnCe/HZSM-5 catalysts with different SiO_2/Al_2O_3 ratio. As presented in Fig. 1**a**, the bands at 1447 and 1607 cm^{-1} were corresponded with pyridine adsorbed on Lewis acid sites, and the bands at 1543 and 1635 cm^{-1} were related to pyridine adsorbed on Brønsted acid sites. The band at 1490 cm^{-1} was assigned to Brønsted and Lewis acid sites [22,23]. The quantitative results of Py-IR spectra were summarized in Table 1. MnCe/HZSM5-25 had the largest amounts of B, L and total acid sites (0.065, 0.143, 0.208 mmol/g) compared with MnCe/HZSM5-100 (0.016, 0.120, 0.136 mmol/g), MnCe/HZSM5-360 (0.014, 0.087, 0.101 mmol/g) and MnO_x-CeO_2 (0.013, 0.041, 0.054 mmol/g). The solid acid HZSM-5 with

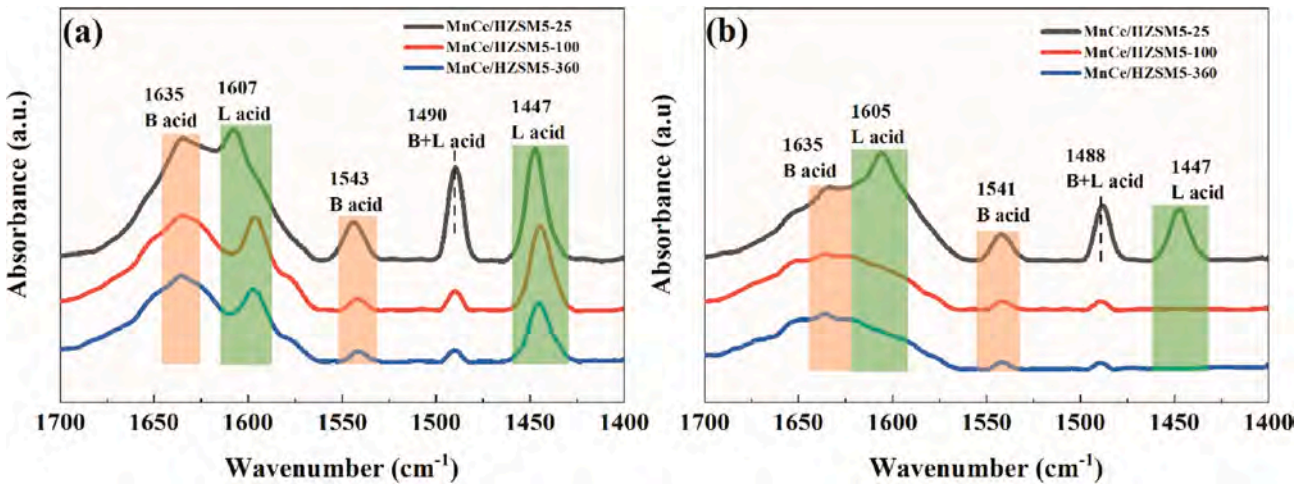

Fig. 1. Py-IR spectra of MnCe/HZSM-5 catalysts after desorption of pyridine at (a) 200 °C and (b) 350 °C.

Table 1
Information obtained from Py-IR spectra and XPS spectra of catalysts.

Sample	Py-IR results (200 °C)		Py-IR results (350 °C)		XPS results		
	B acid sites (mmol/g)	L acid sites (mmol/g)	B acid sites (mmol/g)	L acid sites (mmol/g)	Mn^{4+}/Mn (%)	Ce^{3+}/Ce (%)	O_{sur}/O (%)
MnCe/HZSM5-25	0.065	0.143	0.044	0.068	31.8	20.5	37.4
MnCe/HZSM5-100	0.016	0.120	0.012	0.000	30.6	19.0	19.7
MnCe/HZSM5-360	0.014	0.087	0.009	0.000	28.2	18.6	15.4

abundant acid sites (Brønsted and Lewis) could adequately promote the acidity of MnO_x-CeO_2 catalyst. Moreover, the Lewis acid sites of MnCe/HZSM-5 catalysts were dominant, while the HZSM-5 was dominated by Brønsted acid sites, indicating that ion exchange between Mn/Ce and HZSM-5 occurred, which transferred the Brønsted acid sites into Lewis acid sites [19,24]. The similar rules were observed in the Py-IR spectra recorded after desorption of pyridine at 350 °C (Fig. 1**b**). The amount of medium and strong acid sites on MnCe/HZSM5-25 was also significantly larger than the others, especially for the L acid sites. In NH_3-SCR reaction, NH_3 is firstly adsorbed on the Brønsted or Lewis acid sites of catalysts, then reacted with gaseous NO or adsorbed NO species. More acid sites are beneficial for the adsorption and activation of NH_3, which may lead to an enhanced catalytic activity [1,2,14].

The valence states of elements on the catalyst surface were evaluated by XPS. The spectra of Mn 2p, Ce 3d and O 1 s were collected in Fig. 2 and the corresponding surface composition information was illustrated in Table 1. The Mn 2p XPS spectra (Fig. 2**a**) were divided into three peaks. The binding energies at 641.8 eV and 643.8 eV were assigned to Mn^{4+} and Mn^{3+}, respectively [25]. The ratio of Mn^{4+}/Mn showed a decreasing trend with the increasing SiO_2/Al_2O_3 ratio. The lower molar ratio of SiO_2/Al_2O_3 is related to larger amount of acid sites, which may benefit for the conversion of Mn species to a high oxidation state (Mn^{4+}) [26]. The Ce 3d XPS spectra (Fig. 2**b**) were consisted of four pairs of spin–orbit doublets including 8 peaks [27]. The peaks labeled as v1 and u1 represent the $3d^{10}4f^1$ initial electronic state corresponding to Ce^{3+}, whereas the other peaks represent the $3d^{10}4f^0$ state belonging to Ce^{4+}. A lower SiO_2/Al_2O_3 ratio of HZSM-5 support had a larger Ce^{3+} proportion, resulting from the reduction of Ce^{4+} to Ce^{3+}. Combining with the Mn composition, the electron transfer between Mn^{3+} and Ce^{4+} ($Mn^{3+} + Ce^{4+} \leftrightarrow Mn^{4+} + Ce^{3+}$) may occur, which increased the Mn^{4+} and Ce^{3+} concentrations. The formation of Ce^{3+} could promote the catalytic activity by creating a charge imbalance, oxygen vacancies and unsaturated chemical bonds on the catalyst surface. The O 1 s XPS spectra (Fig. 2**c**) were deconvoluted into three peaks at 529.5, 531.7 and 532.8 eV, which were ascribed to lattice oxygen (denoted as O_{lat}), surface chemisorbed oxygen (denoted as O_{sur}), and hydroxyl species or adsorbed water (denoted as O_{ads}), respectively [19,27,28]. The surface chemisorbed oxygen O_{sur} was beneficial for both toluene oxidation and SCR process due to its higher mobility than lattice oxygen (O_{lat}) [27,29,30]. The highest O_{sur} percent of 37.4% was identified for MnCe/HZSM5-25 due to

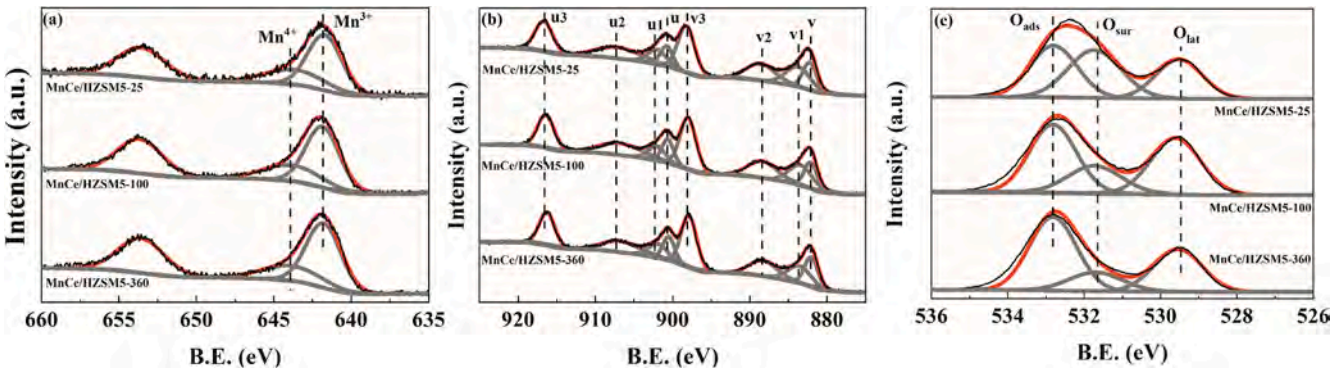

Fig. 2. XPS spectra of (a) Mn 2p, (b) Ce 3d and O 1 s.

its large amount of surface Ce^{3+}, which caused the increase of chemisorbed oxygen from the continuous replenishment of oxygen vacancies upon the uptake of gas-phase O_2 to maintain electric neutrality (e.g., $Ce^{3+} + O_2 \rightarrow O_2^- + Ce^{4+}$) [31]. In conclusion, MnCe/HZSM5-25 has higher concentrations of Mn^{4+}, Ce^{3+} and active surface oxygen.

3.2. Catalytic performance

The SCR and toluene catalytic oxidation reactions of MnCe/HZSM-5 catalysts and MnCe/γ-Al_2O_3 (for comparison purpose) were carried out to test the simultaneous removal potential. T_{50} and T_{90} (the temperature when NO conversion was 50% or 90%) were used to evaluate the SCR activity (Fig. 3**a**). The T_{50} of MnCe/HZSM-5 catalysts (146–173 °C) was higher than MnCe/γ-Al_2O_3 (115 °C), indicating that MnCe/γ-Al_2O_3 possessed relatively higher SCR activity at low temperature range (<200 °C). This result was further confirmed by kinetic analysis (Fig. 3**b**). A lowest activation energy (E_a) of 9.96 kJ/mol on MnCe/γ-Al_2O_3 was identified. However, an opposite rule was observed for T_{90}. The T_{90} of MnCe/HZSM-5 catalysts (205–256 °C) were significantly lower than MnCe/γ-Al_2O_3 (282 °C). Among them, the MnCe/HZSM5-25 had the lowest T_{90} of 205 °C and the widest temperature range of 200–400 °C with NO conversion > 80%. Besides, the N_2 selectivity of the MnCe/HZSM-5 catalysts was much superior than our previous research on MnO_x-CeO_2 catalyst (~50% at 250 °C) [1] resulting from the positive effect of HZSM-5 support with abundant acid sites [24]. Especially, the N_2 selectivity of MnCe/HZSM5-25 was above 96% in the whole testing temperature range of 50–400 °C (Fig. 3**c**).

In the meantime, MnCe/HZSM-5 catalysts showed excellent toluene catalytic oxidation activity (Fig. 3**d**). Almost 100% conversion was achieved for all catalysts at temperatures above 300 °C. The toluene conversions of MnCe/HZSM-5 catalysts were higher than MnCe/γ-Al_2O_3. Especially, MnCe/HZSM5-25 converted more than 64% of toluene at 200 °C. Combining with the catalyst characterization results, MnCe/HZSM5-25 was the optimal catalyst for the removal of NO_x and toluene with broad temperature window and pretty high N_2 selectivity due to higher acidity and more Mn^{4+}, Ce^{3+} and active surface oxygen.

3.3. Impact of toluene poisoning

3.3.1. SCR activity

The simultaneous abatement of NO_x and toluene on the optimal MnCe/HZSM5-25 was afterwards conducted to study the impact of toluene on NH_3-SCR performance. During this process, the toluene conversion maintained above 60% in 200–400 °C (**Fig. S3**). However, as presented in Fig. 4**a**, the addition of toluene showed a negative effect on SCR activity, which considerably inhibited the NO conversion. This inhibition was more obvious with higher toluene concentrations or at higher temperatures (**Fig. S4**). The same phenomenon was overserved over MnCe/HZSM5-100 and MnCe/HZSM5-360 catalysts in **Fig. S5**. An increase of T_{50} by 14 °C and a decrease of NO conversion by 18.9% at 250 °C were quantified. In the meantime, the N_2 selectivity exhibited insignificant change. A 14 h long-term test at 250 °C (2 h SCR + 6 h SCR with toluene + 6 h SCR) was then carried out to investigate the NH_3-SCR deactivation process induced by toluene (Fig. 4**b**). The NO conversion

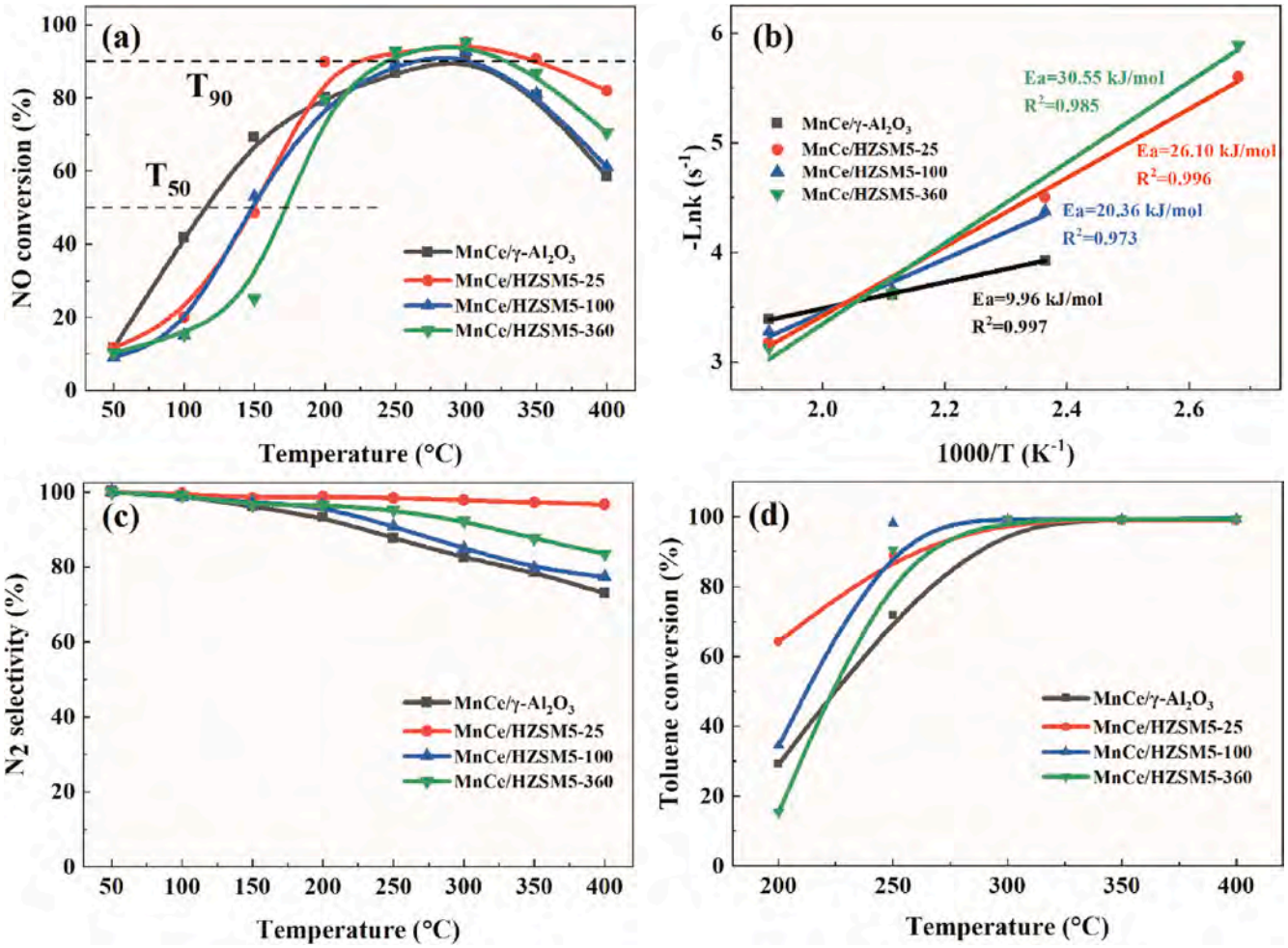

Fig. 3. (a) NO conversion, (b) Arrhenius plots and (c) N_2 selectivity in NH_3-SCR reaction, and (d) toluene conversion on MnCe/HZSM-5 catalysts. Reaction conditions: 500 ppm NH_3 and 500 ppm NO for (a)-(c). 50 ppm toluene for (d). 10 vol% O_2, Q = 200 mL/min and GHSV = 60,000 mL/(g·h) for (a)-(d).

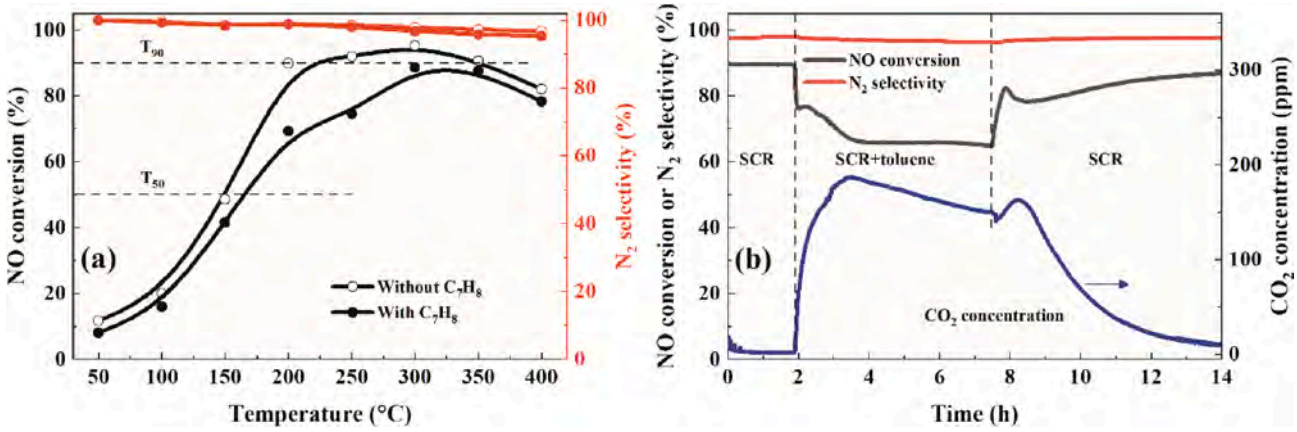

Fig. 4. (a) NO conversion and N_2 selectivity (b) long-term experiment (T = 250 °C) on MnCe/HZSM-5 in simultaneous removal process. Reaction conditions: 500 ppm NH_3, 500 ppm NO, 50 ppm toluene (when used), 10 vol% O_2, Q = 200 mL/min, GHSV = 60,000 mL/(g·h).

and N_2 selectivity in initial SCR stage were quite stable. When 50 ppm toluene was added, the NO conversion dropped quickly and reached a new stable state. After toluene flow was cut off, the NO conversion recovered gradually, suggesting that the deactivation was reversible. During this process, the CO_2 concentration was still higher than 100 ppm for 2 h because of the semivolatile byproducts on the catalyst surface derived from the toluene oxidation, which covered the active sites and obstructed the pores, subsequently resulted in the catalyst deactivation. The ~7% weight loss of used catalyst in TGA result and the exothermic DSC curve in Fig. S6 further demonstrated the formation of coke. In fact,

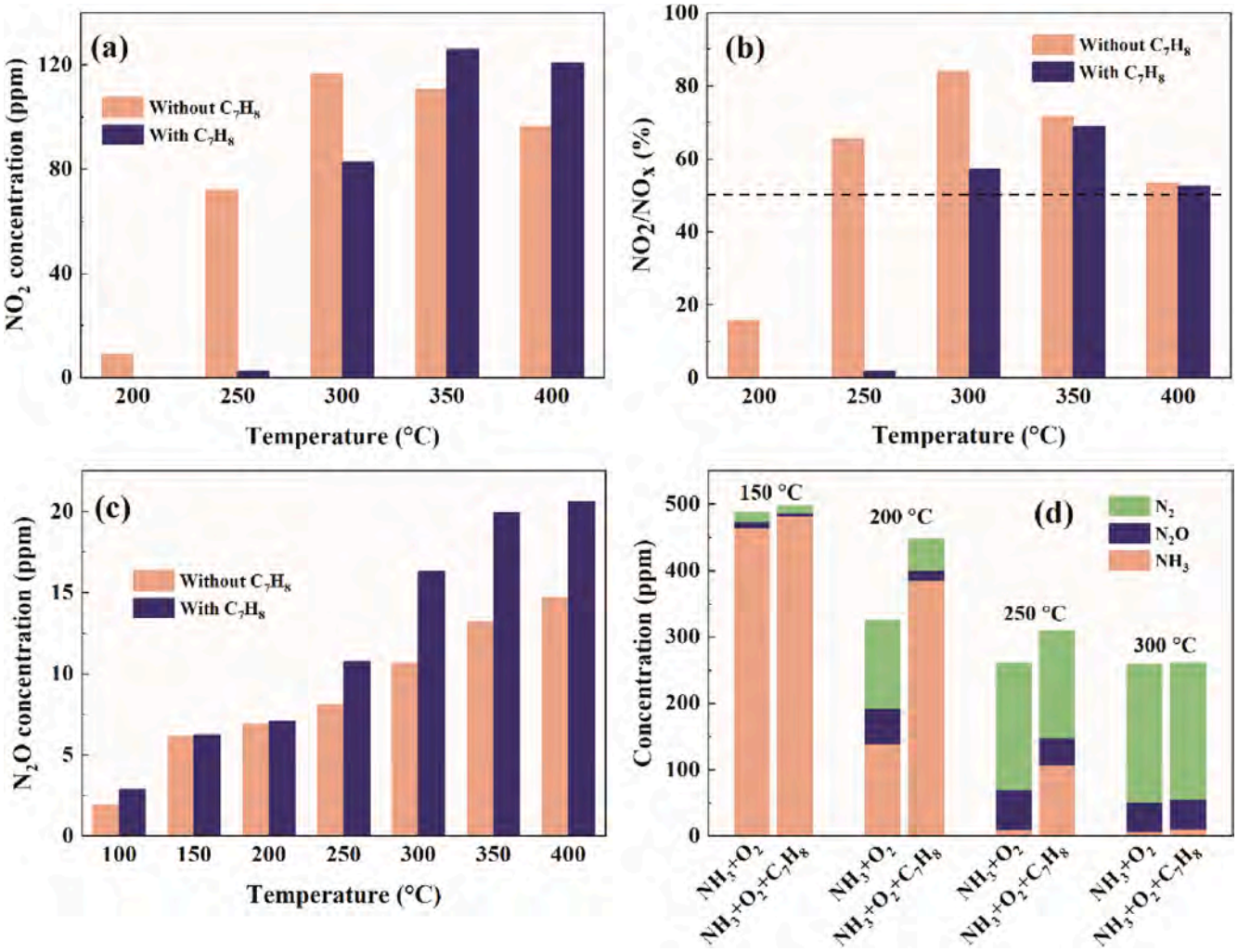

Fig. 5. Effect of toluene on (a) NO_2 concentration, (b)NO_2/NO_x ratio, (c) N_2O concentration in SCR reaction, and (d) product concentration in C-O reaction. Reaction conditions: 500 ppm NH_3, 500 ppm NO and 50 ppm toluene (when used) for (a)-(c). 500 ppm NH_3 and 50 ppm toluene (when used) for (d). 10 vol% O_2, Q = 200 mL/min and GHSV = 60,000 mL/(g·h) for (a)-(d).

the solid acid supports with rich porosity and high stability benefit the catalytic activity, but face the coke deactivation problem due to strong acidity [32].

3.3.2. SCR side reactions

During SCR process, side reactions such as non-selective catalytic reduction (NSCR, e.g., $4NH_3 + 4NO + 3O_2 \rightarrow 4N_2O + 6H_2O$), NH_3 catalytic oxidation (C-O, e.g., $2NH_3 + 2O_2 \rightarrow N_2O + 3H_2O$), and NO catalytic oxidation (NOCO, $2NO + O_2 \rightarrow 2NO_2$) occur and produce inevitable byproducts NO_2 and N_2O. The NO_2 concentration was only 8.8 ppm at 200 °C, whereas a noticeable amount of NO_2 (72.2–116.5 ppm) was produced at 250–400 °C (Fig. 5**a**). The presence of toluene dramatically inhibited the NO to NO_2 oxidation at 250 °C, resulting in a decrease of NO_2/NO_x ratio from 65.6% to 1.7% (Fig. 5**b and Fig. S7**), which reduced the percentage of "fast SCR" process [3,33].

As one of the major concerns of Mn-based SCR catalysts, byproduct greenhouse gas N_2O is mainly generated from NSCR and NH_3 catalytic oxidation (denoted as C-O). The total N_2O concentration was 1.4–14.7 ppm in NH_3-SCR reaction. And toluene had negligible impact on the total N_2O concentration (Fig. 5**(c)**). In the meantime, the influence of toluene on the C-O was further studied (Fig. 5**(d)**). N_2 was the major product of C-O. A small amount of N_2O was generated. NO was barely produced (**Fig. S8**). NH_3 conversion and $N_2 + N_2O$ formation were obviously suppressed by toluene, leading to less NH_2 species generated by the NH_3 oxidation (e.g., $NH_3 + O \rightarrow NH_2 + OH$) on the catalyst surface. Since NH_2 species are key intermediates in NH_3-SCR reaction [28] the inhibition of NH_2 formation resulted in the decline of SCR activity.

3.3.3. Adsorption states

TPD experiments were done to investigate the effect of toluene on the adsorption–desorption behaviors of reactants. The NH_3 desorption band (without toluene) was very broad within 150–450 °C (Fig. 6**a**) and could be divided into two peaks at 100–300 °C and 300–500 °C, which corresponded to the NH_3 adsorption on weak/middle acid sites (Lewis acid sites) and strong acid sites (Brønsted acid sites), respectively [2,34]. Obviously, NH_3 could be adsorbed on both L and B acid sites of MnCe/HZSM-5. The presence of toluene increased the NH_3 adsorption capacity from 821.4 to 1759.5 μmol/g (Table 2). The NH_3 desorption amounts without and with toluene were 459.5 and 1623.5 μmol/g, respectively. Thus, the NH_3 conversion without and with toluene were calculated as 44.1% and 7.7%, respectively. Obviously, toluene still restrained the NH_3 oxidation by surface oxygen. The desorption products of NH_3-TPD were shown in Fig. 6**b** and Table 2·NH_3 could be oxidized by surface oxygen on catalyst to form N_2, N_2O and NO. The concentration of NO was higher than N_2O, which was opposite from C-O. The oxidation of NH_3 by surface oxygen and gaseous O_2 may undergo different routes. Moreover, the desorption temperature of TPD (50–650 °C) was higher than C-O. Higher temperatures were beneficial for the NO yield. Similar

Table 2
Quantitative analysis of TPD results (μmol/g).

	$NH_{3(ads)}$ or $NO_{(ads)}$	NH_3	N_2O	NO	NO_2
NH_3-TPD	821.4	459.5	2.0	31.6	/
$NH_3 + C_7H_8$-TPD	1759.5	1623.5	0.7	45.2	/
$NO + O_2$-TPD	289.8	/	/	96.3	193.5
$NO + O_2 + C_7H_8$-TPD	257.1	/	/	201.0	56.1

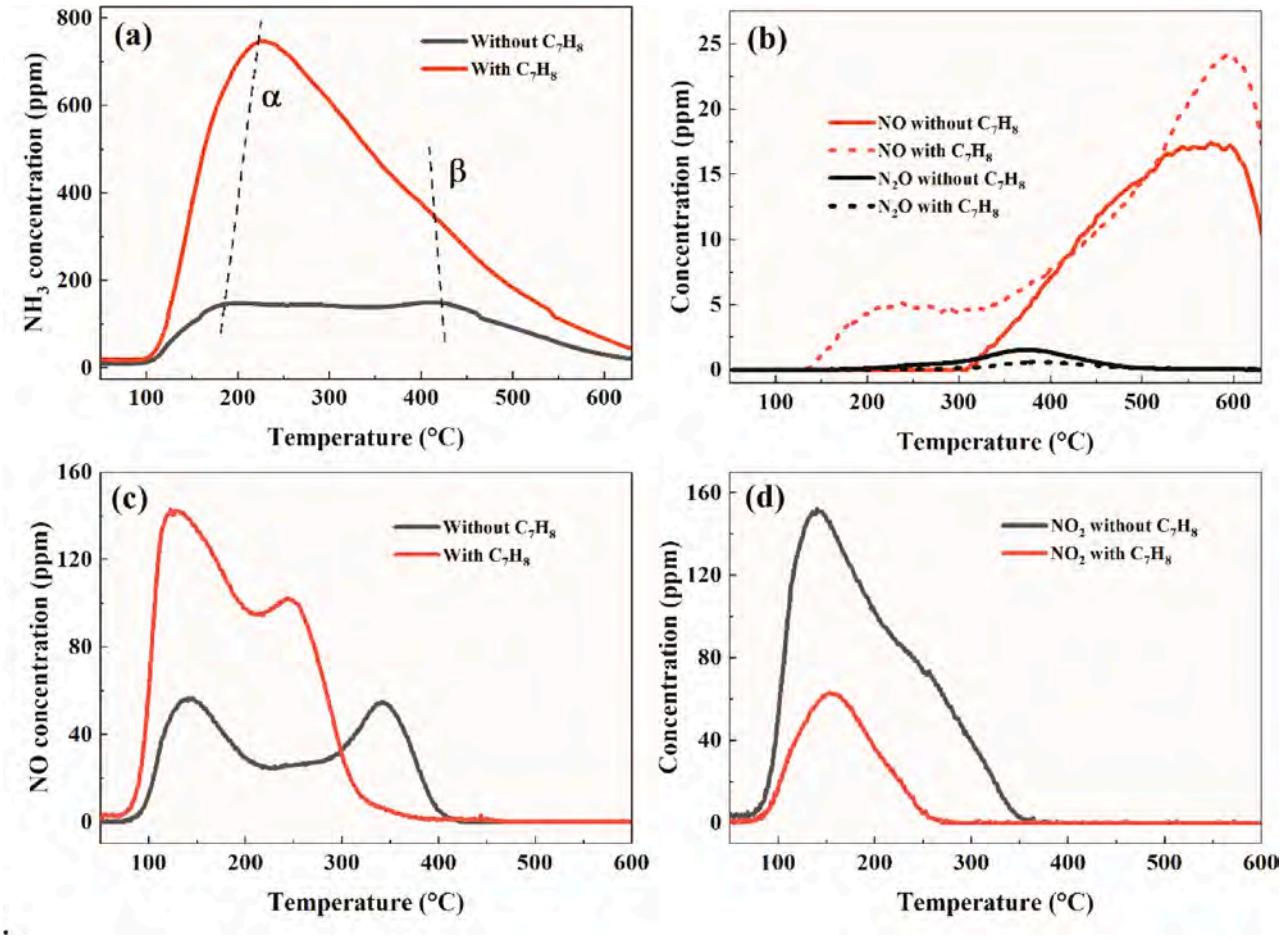

Fig. 6. Effect of toluene on (a) NH_3-TPD and (b) desorption products of NH_3-TPD, (c) $NO + O_2$-TPD and (d) desorption products of $NO + O_2$-TPD.

with C-O, the NO formation was slightly enhanced, while the yield of N_2 + N_2O was decreased more significantly. The amount of surface oxygen on catalyst was fixed, large proportion of which was consumed by toluene during the desorption process to form CO_2 (**Fig. S9**). So less oxygen was available to oxidize NH_3.

As for the NO + O_2-TPD (Fig. 6**c, d**), toluene decreased the NO adsorption capacity and NO oxidation product NO_2 from 289.8 and 193.5 to 257.1 and 56.1 μmol/g, respectively. This further confirmed the inhibition effect of toluene on NO oxidation.

The NH_3, NO_x and toluene adsorption intermediate species and their interactions were measured by *in situ* DRIFTs and the results were presented in Figs. 7 and 8. Several bands at wavenumber range of 1000–2000 cm^{-1} were observed after the adsorption of NH_3 on the catalyst surface (Fig. 7**a**). The bands at 1732, 1606, 1471, 1182 and 1033 cm^{-1} were related to the coordinated NH_3 on the L acid sites [1,35]. The band at 1546 cm^{-1} was assigned to the ionic NH_4^+ on B acid sites [35,36]. As for toluene adsorption (Fig. 7**b**), the band at 1625 cm^{-1} corresponded to benzaldehyde species (C=O) resulted from the oxidation of toluene adsorption intermediates. The bands centered at 1591 and 1573 cm^{-1} were related to the skeleton stretching vibrations of the aromatic ring. The bands at 1490 and 1365 cm^{-1} could be denoted as the asymmetric methyl bending vibrations and bending vibrations of methylene group, respectively [37].

The spectra of the co-adsorption of NH_3 and toluene at 1000–2000 cm^{-1} were similar with that of NH_3 (Fig. 7**c**). Most bands of toluene adsorption species were overlapped. Surprisingly, a strong new band at 2233 cm^{-1} appeared, which was related to the C≡N bond in nitriles (e.g., C_6H_5CN) [4]. The benzonitrile was generated from the reaction between NH_3 and C_7H_8 with the participation of active surface oxygen (O*) (e.g., $C_6H_5CH_3 + NH_3 + 3O^* \rightarrow C_6H_5CN + 3H_2O$) [4]. To further investigate the influence of toluene on NH_3 adsorption intermediates, NH_3 was passed on the toluene pre-adsorbed catalyst (Fig. 7**d**). The

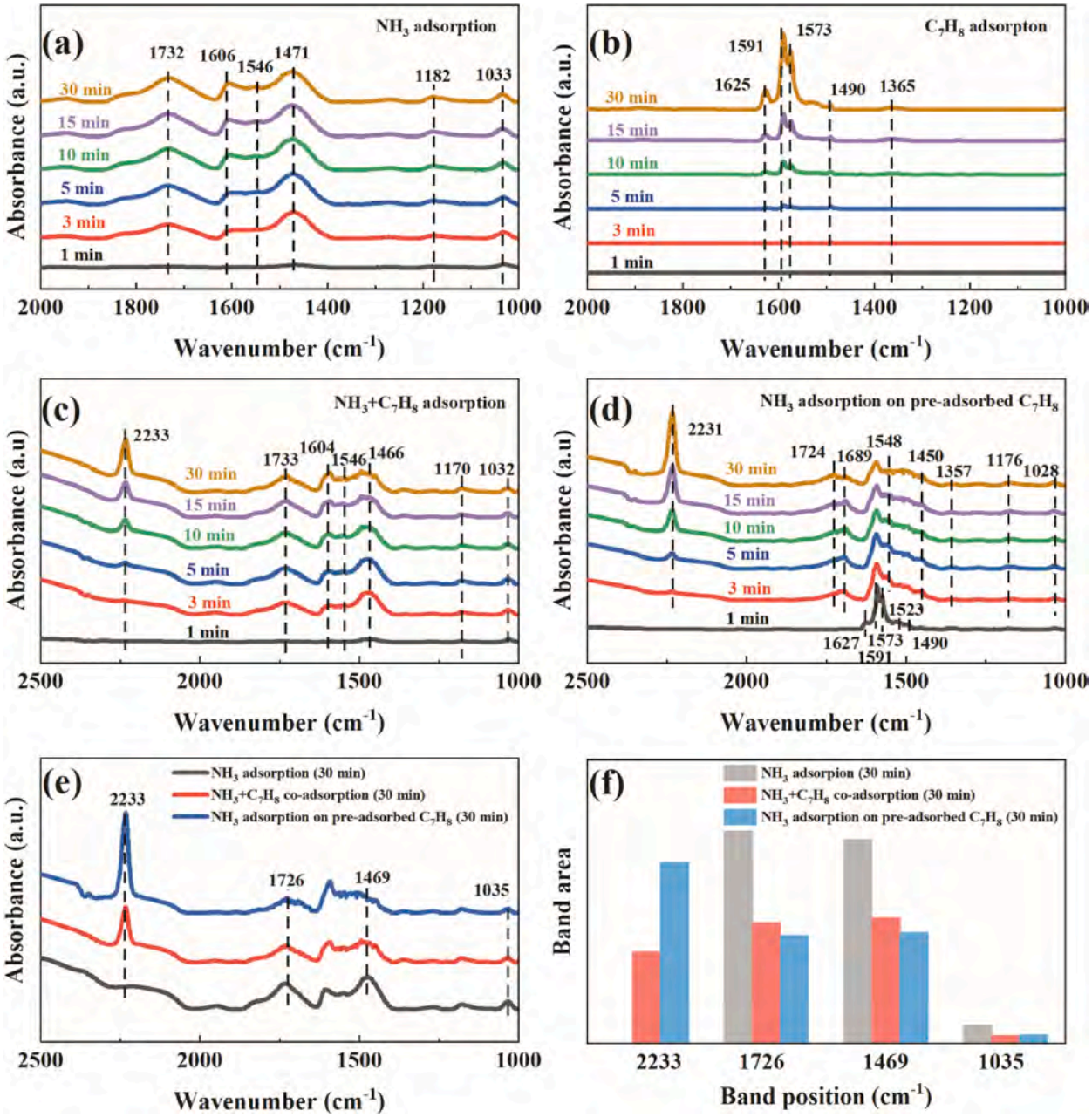

Fig. 7. *In situ* DRIFTs spectra recorded at 250 °C of (a) NH_3 adsorption, (b) toluene adsorption, (c) NH_3 + toluene co-adsorption, (d) NH_3 adsorption on toluene pre-adsorbed catalyst, and (e, f) comparison of NH_3 adsorption, NH_3 + toluene co-adsorption and NH_3 adsorption on toluene pre-adsorbed catalyst.

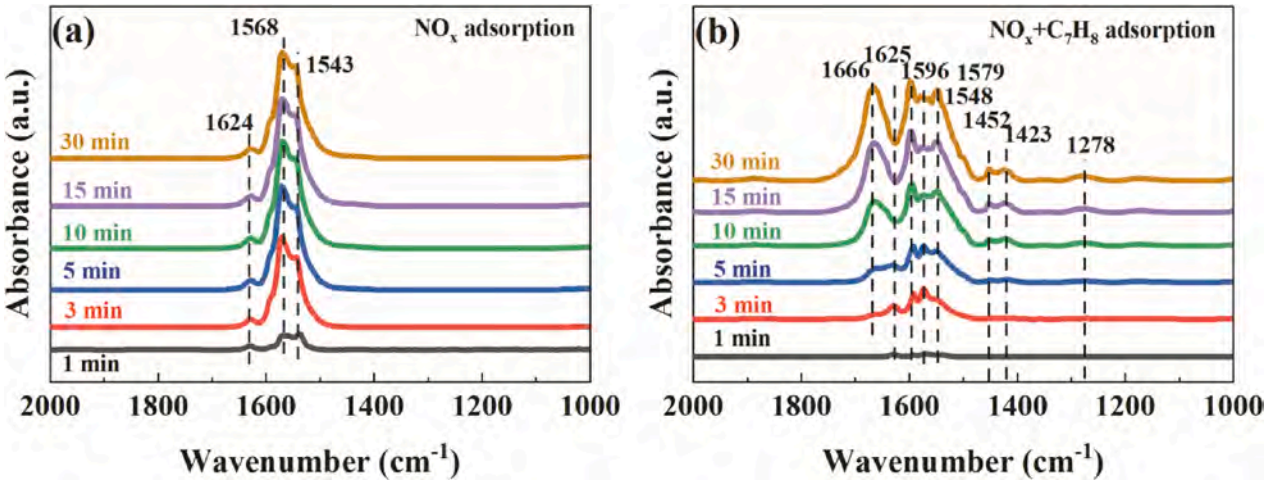

Fig. 8. *In situ* DRIFTs spectra recorded at 250 °C of (a) NO + O_2 adsorption, and (b) NO + O_2 + toluene co-adsorption.

intensities of bands at 1627, 1591, and 1573 cm^{-1} related to the toluene adsorption species decreased, whereas the nitriles at 2231 cm^{-1} gradually increased. The pre-adsorbed toluene was consumed by NH_3, which further proved the existence of reaction between toluene and NH_3. Moreover, a new band at 1689 cm^{-1} corresponding to the ionic NH_4^+ on B acid sites appeared. We also compared the spectra of NH_3 adsorption, NH_3 + toluene co-adsorption and NH_3 adsorption on toluene pre-adsorbed catalyst in Fig. 7**e, f**. The co-adsorption of toluene decreased the areas of bands at 1726, 1469 and 1035 cm^{-1} corresponding to the coordinated NH_3 on L acid sides, which was believed to be active in NH_3-SCR reaction. On the contrary, the area of band at 2233 cm^{-1} (nitriles) increased to 1.129–2.231. The byproduct nitriles not only decreased the available NH_3 in SCR reaction, but also occupied the active sites on catalyst surface. Therefore, although toluene enhanced the catalyst acidity and NH_3 adsorption capacity (TPD result), the inactive NH_4^+ on B acid sites, and the formation of nitriles that decreased the active coordinated NH_3 on L acid sides, contributed to a lower SCR activity.

After the adsorption of NO + O_2, three bands at 1624, 1568 and 1543 cm^{-1} were presented (Fig. 8**a**). The band at 1624 cm^{-1} was ascribed to adsorbed NO_2 species, while the bands at 1568 and 1543 cm^{-1} could be ascribed to bidentate nitrates [2]. The bands corresponding to monodentate nitrate, linear nitrite and chelating nitrite were not detected at the testing temperature of 250 °C due to their poor thermal stability [38]. The abundant O_{sur} on MnCe/HZSM-5 contributed to the formation of nitrate species and NO_2-containing species. As reported [39] the gaseous O_2 could accept electron from Ce^{3+} to form O* and Ce^{4+}. The Ce^{4+} could be then reduced to Ce^{3+} by neighboring Mn^{3+}, which increased more oxygen vacancies and surface active O* that oxidizes NO to NO_2* and NO_3* species [38]. Different from NH_3, the spectra of co-adsorption of NO + O_2 and toluene more liked the combination of the individual spectra (Fig. 8**b**). The DRIFTs spectra proved again that toluene inhibited the NO_x adsorption capacity. Besides, the new bands at 1423–1452 and 1278 cm^{-1} were related to the linear nitrite and chelating nitrite, respectively [40,41]. The formation of nitrite species indicated that toluene inhibited the NO oxidizing ability of MnCe/HZSM-5 catalyst, which was consistent with the inhibitory impacts of toluene on SCR side reactions (NO oxidation and NH_3 oxidation)

3.3.4. *Transient reactions*

During NH_3-SCR reaction, the adsorbed NH_x species react with either gaseous NO_x following Eley-Rideal (E-R) mechanism or adsorbed NO_x species following Langmuir-Hinshelwood (L-H) mechanism to generate NH_3-NO_x that decomposes to N_2 and H_2O [14,35,38]. When passing NO + O_2 onto the NH_3 pre-adsorbed catalyst, the coordinated NH_3 on L acid sites were rapidly consumed within 10 min, whereas the ionic NH_4^+ on B acid sites (1540 cm^{-1}) changed insignificantly (Fig. 9**a**). The coordinated NH_3 is active in SCR reaction through E-R mechanism, and ionic NH_4^+ is inactive. The adsorbed NH_2/NH_3 species then reacted with gaseous NO to form intermediate NH_2-NO or NH_3-NO which decomposed to N_2 and H_2O. When passing NH_3 onto the NO + O_2 pre-adsorbed catalyst (Fig. 9**b**), the bands intensities of adsorbed NO_x (1568, 1540 cm^{-1}) in the IR spectra showed no obvious change, suggesting that adsorbed NH_3 may not react with adsorbed NO_x (L-H mechanism). Thus, we concluded the NH_3-SCR reaction over MnCe/HZSM-5 catalyst predominantly followed E-R mechanism.

To reveal the effect of toluene on the transient reaction, NO + O_2 was introduced into the cell to react with the NH_3 + toluene pre-adsorbed catalyst (Fig. 9**c**). Similarly, the coordinated NH_3 was completely consumed, whereas the band at 1546 cm^{-1} assigned to ionic NH_4^+ didn't change much. In addition, the nitriles at 2233 cm^{-1} slightly decreased, indicating that it was relatively stable and difficult to be further oxidized. On the other hand, when passing NH_3 over NO_x + toluene pre-adsorbed catalyst (Fig. 9**d**), the original bands maintained. The pre-adsorbed NO_x species barely reacted with NH_3. As a consequence, the dominant E-R mechanism in NH_3-SCR is not influenced by toluene.

4. Conclusions

In this work, the NO_x and toluene were simultaneously removed over MnCe/HZSM-5 catalysts, which possessed higher activities than MnCe/γ-Al_2O_3. Taking the advantage of HZSM-5, the MnCe/HZSM5-25 catalyst exhibited broad window and excellent N_2 selectivity that were much better than MnO_x-CeO_2 catalyst in NH_3-SCR reaction. HZSM-5 provided more acid sites especially Lewis acid due to the ion exchange between Mn/Ce and HZSM-5 that transferred the Brønsted acid into Lewis acid. We demonstrated the great potential of HZSM-5 modified MnO_x-CeO_2 catalysts for the NO_x and toluene co-removal. However, a reversible deactivation over MnCe/HZSM-5 in NH_3-SCR occurred in the presence of toluene, while the dominant E-R reaction mechanism could not be influenced. The impacts of toluene poisoning include (1) formation of coke covered the active sites and pores, especially the distinct byproduct nitriles (–CN) from the reaction between toluene and NH_3; (2) inhibition of "fast SCR" by suppressing NO oxidation to NO_2; (3) limitation of active NH_2 species generation by weakening the NH_3 oxidizing/activating ability of catalyst.

Declaration of Competing Interest

The authors declare that they have no known competing financial interests or personal relationships that could have appeared to influence

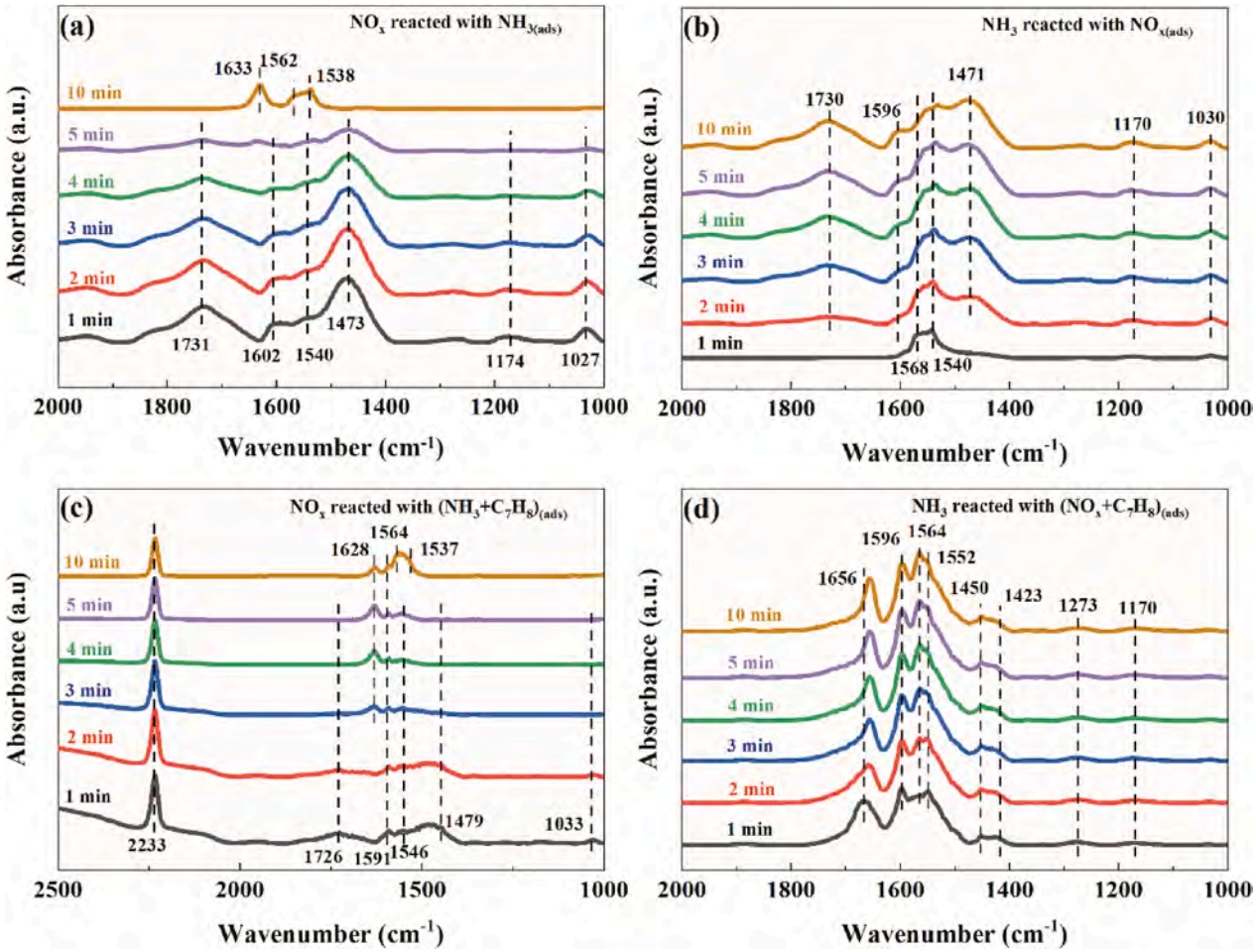

Fig. 9. *In situ* DRIFTs spectra recorded at 250 °C of (a) passing NO + O_2 over NH_3 pre-adsorbed catalyst, (b) passing NH_3 over NO + O_2 pre-adsorbed catalyst, (c) passing NO + O_2 over NH_3 + toluene pre-adsorbed catalyst, and (d) passing NH_3 over NO + O_2 + toluene pre-adsorbed catalyst.

the work reported in this paper.

Acknowledgments

This work was financially supported by the Central Public-interest Scientific Institution Basal Research Fund (PM-zx703-202002-015), and the National Key Research and Development Plan of China (2019YFC0214300).

Appendix A. Supplementary data

Supplementary data to this article can be found online at https://doi.org/10.1016/j.cej.2021.128838.

References

[1] L. Ye, P. Lu, X. Chen, P. Fang, Y. Peng, J. Li, H. Huang, The deactivation mechanism of toluene on MnO_x-CeO_2 SCR catalyst, Appl. Catal. B Environ. 277 (2020), 119257.

[2] L. Zhao, Y. Huang, J. Zhang, L. Jiang, Y. Wang, Al_2O_3-modified CuO-CeO_2 catalyst for simultaneous removal of NO and toluene at wide temperature range, Chem. Eng. J. 397 (2020), 125419.

[3] L. Gan, W. Shi, K. Li, J. Chen, Y. Peng, J. Li, Synergistic promotion effect between NO_x and chlorobenzene removal on MnO_x–CeO_2 catalyst, ACS Appl. Mater. Interfaces 10 (36) (2018) 30426–30432.

[4] W. Jiang, Y. Yu, F. Bi, P. Sun, X. Weng, Z. Wu, Synergistic elimination of NO_x and chloroaromatics on a commercial V_2O_5-WO_3/TiO_2 catalyst: Byproduct analyses and the SO_2 effect, Environ. Sci. Technol. 53 (2019) 12657–12667.

[5] D. Wang, J. Chen, Y. Peng, W. Si, X. Li, B. Li, J. Li, Dechlorination of chlorobenzene on vanadium-based catalysts for low-temperature SCR, Chem. Commun. 54 (16) (2018) 2032–2035.

[6] Q. Wang, P.C. Hung, S. Lu, M.B. Chang, Catalytic decomposition of gaseous PCDD/Fs over V_2O_5/TiO_2-CNTs catalyst: Effect of NO and NH_3 addition, Chemosphere 159 (2016) 132–137.

[7] F. Bertinchamps, M. Treinen, P. Eloy, A.-M. Dos Santos, M.M. Mestdagh, E. M. Gaigneaux, Understanding the activation mechanism induced by NO_x on the performances of VO_x/TiO_2 based catalysts in the total oxidation of chlorinated VOCs, Appl. Catal. B 70 (1-4) (2007) 360–369.

[8] F. Bertinchamps, M. Treinen, N. Blangenois, E. Mariage, E. Gaigneaux, Positive effect of NO_x on the performances of VO_x/TiO_2-based catalysts in the total oxidation abatement of chlorobenzene, J. Catal. 230 (2005) 493–498.

[9] L. Gan, K. Li, S. Xiong, Y. Zhang, J. Chen, Y. Peng, J. Li, MnO_x-CeO_2 catalysts for effective NO_x reduction in the presence of chlorobenzene, Catal. Commun. 117 (2018) 1–4.

[10] L. Gan, Y.u. Wang, J. Chen, T. Yan, J. Li, J. Crittenden, Y. Peng, The synergistic mechanism of NO_x and chlorobenzene degradation in municipal solid waste incinerators, Catal. Sci. Technol. 9 (16) (2019) 4286–4292.

[11] C. Fan, K. Li, Y. Peng, R. Duan, F. Hu, Q. Jing, J. Chen, J. Li, Fe-Doped α-MnO_2 nanorods for the catalytic removal of NO_x and chlorobenzene: The relationship between lattice distortion and catalytic redox properties, Phys. Chem. Chem. Phys. 21 (2019) 25880–25888.

[12] G. Su, L. Huang, S. Liu, H. Lu, F. Yang, M. Zheng, The combined disposal of 1,2,4-trichlorobenzene and nitrogen oxides using the synthesized $Ce_{0.2}TiAl_\alpha O_x$ micro/nanomaterial, Catal. Sci. Technol. 5 (2) (2015) 1041–1051.

[13] C. He, J. Cheng, X. Zhang, M. Douthwaite, S. Pattisson, Z. Hao, Recent advances in the catalytic oxidation of volatile organic compounds: a review based on pollutant sorts and sources, Chem. Rev. 119 (2019) 4471–4568.

[14] L. Han, S. Cai, M. Gao, J. Hasegawa, P. Wang, J. Zhang, L. Shi, D. Zhang, Selective catalytic reduction of NO_x with NH_3 by using novel catalysts: state of the art and future prospects, Chem. Rev. 119 (2019) 10916–10976.

[15] Y. Shu, M. He, J. Ji, H. Huang, S. Liu, D.Y.C. Leung, Synergetic degradation of VOCs by vacuum ultraviolet photolysis and catalytic ozonation over Mn-xCe/ZSM-5, J. Hazard. Mater. 364 (2019) 770–779.

[16] R. Yan, S. Lin, Y. Li, W. Liu, Y. Mi, C. Tang, L. Wang, P. Wu, H. Peng, Novel shielding and synergy effects of Mn-Ce oxides confined in mesoporous zeolite for low temperature selective catalytic reduction of NO_x with enhanced SO_2/H_2O tolerance, J. Hazard. Mater. 396 (2020), 122592.

[17] J. Shao, S. Cheng, Z. Li, B. Huang, Enhanced catalytic performance of hierarchical MnO_x/ZSM-5 catalyst for the low-temperature NH_3-SCR, Catalysts. 10 (2020) 311.
[18] G. Carja, Y. Kameshima, K. Okada, C.D. Madhusoodana, Mn–Ce/ZSM5 as a new superior catalyst for NO reduction with NH_3, Appl. Catal. B 73 (1-2) (2007) 60–64.
[19] X. Weng, P. Sun, Y. Long, Q. Meng, Z. Wu, Catalytic oxidation of chlorobenzene over $Mn_xCe_{1-x}O_2$/HZSM-5 catalysts: a study with practical implications, Environ. Sci. Technol. 51 (2017) 8057–8066.
[20] P. Sun, W. Wang, X. Dai, X. Weng, Z. Wu, Mechanism study on catalytic oxidation of chlorobenzene over $Mn_xCe_{1-x}O_2$/H-ZSM5 catalysts under dry and humid conditions, Appl. Catal. B 198 (2016) 389–397.
[21] P. Lu, Q. Huang, A.C. (Thanos) Bourtsalas, Y. Chi, J. Yan, Experimental research of basic properties and reactivity of waste derived chars, Appl. Therm. Eng. 119 (2017) 639–649.
[22] C.A. Emeis, Determination of integrated molar extinction coefficients for infrared absorption bands of pyridine adsorbed on solid acid catalysts, J. Catal. 141 (2) (1993) 347–354.
[23] T. Yashima, Infrared study of cation-exchanged mordenites and Y faujasites adsorbed with ammonia and pyridine, J. Catal. 27 (2) (1972) 329–333.
[24] T. Zhang, J. Liu, D. Wang, Z. Zhao, Y. Wei, K. Cheng, G. Jiang, A. Duan, Selective catalytic reduction of NO with NH_3 over HZSM-5-supported Fe–Cu nanocomposite catalysts: The Fe–Cu bimetallic effect, Appl. Catal. B 148-149 (2014) 520–531.
[25] F. Cao, J. Xiang, S. Su, P. Wang, S. Hu, L. Sun, Ag modified Mn–Ce/γ-Al_2O_3 catalyst for selective catalytic reduction of NO with NH_3 at low-temperature, Fuel Process. Technol. 135 (2015) 66–72.
[26] H. Wang, B. Peng, R. Zhang, H. Chen, Y. Wei, Synergies of Mn oxidative ability and ZSM-5 acidity for 1, 2-dichloroethane catalytic elimination, Appl. Catal. B Environ. 276 (2020), 118922.
[27] H. Xiaosheng, Z. Guodong, D. Fang, T. Zhicheng, An environmentally friendly wide temperature $CeWTiO_x$ catalyst with superior performance for the selective catalytic reduction NO_x with NH_3, J. Ind. Eng. Chem. 69 (2019) 66–76.
[28] D. Wang, Y. Peng, Q. Yang, S. Xiong, J. Li, J. Crittenden, Performance of modified $La_xSr_{1-x}MnO_3$ perovskite catalysts for NH_3 oxidation: TPD, DFT, and kinetic studies, Environ. Sci. Technol. 52 (2018) 7443–7449.
[29] Y. Liu, W. Yao, X. Cao, X. Weng, Y. Wang, H. Wang, Z. Wu, Supercritical water syntheses of Ce_xTiO_2 nano-catalysts with a strong metal-support interaction for selective catalytic reduction of NO with NH_3, Appl. Catal. B 160-161 (2014) 684–691.
[30] X. Chen, X. Chen, E. Yu, S. Cai, H. Jia, J. Chen, P. Liang, In situ pyrolysis of Ce-MOF to prepare CeO_2 catalyst with obviously improved catalytic performance for toluene combustion, Chem. Eng. J. 344 (2018) 469–479.
[31] X. Lin, S. Li, H. He, Z. Wu, J. Wu, L. Chen, D. Ye, M. Fu, Evolution of oxygen vacancies in MnO_x-CeO_2 mixed oxides for soot oxidation, Appl. Catal. B 223 (2018) 91–102.
[32] C. He, J. Li, J. Cheng, L. Li, P. Li, Z. Hao, Z.P. Xu, Comparative studies on porous material-supported Pd catalysts for catalytic oxidation of benzene, toluene, and ethyl acetate, Ind. Eng. Chem. Res. 48 (15) (2009) 6930–6936.
[33] M. Iwasaki, H. Shinjoh, A comparative study of "standard", "fast" and "NO_2" SCR reactions over Fe/zeolite catalyst, Appl. Catal. A 390 (1-2) (2010) 71–77.
[34] P. Yang, S. Zuo, Z. Shi, F. Tao, R. Zhou, Elimination of 1,2-dichloroethane over $(Ce, Cr)_xO_2/MO_y$ catalysts (M = Ti, V, Nb, Mo, W and La), Appl. Catal. B 191 (2016) 53–61.
[35] S. Xiong, J. Chen, N. Huang, T. Yan, Y. Peng, J. Li, The poisoning mechanism of gaseous HCl on low-temperature SCR catalysts: MnO_x-CeO_2 as an example, Appl. Catal. B Environ. 267 (2020), 118668.
[36] S. Yang, C. Wang, J. Li, N. Yan, L. Ma, H. Chang, Low temperature selective catalytic reduction of NO with NH_3 over Mn–Fe spinel: performance, mechanism and kinetic study, Appl. Catal. B 110 (2011) 71–80.
[37] Y. Wang, H. Arandiyan, Y. Liu, Y. Liang, Y. Peng, S. Bartlett, H. Dai, S. Rostamnia, J. Li, Template-free scalable synthesis of flower-like $Co_{3-x}Mn_xO_4$ spinel catalysts for toluene oxidation, ChemCatChem 10 (16) (2018) 3429–3434.
[38] B. Wang, M. Wang, L. Han, Y. Hou, W. Bao, C. Zhang, G. Feng, L. Chang, Z. Huang, J. Wang, Improved activity and SO_2 resistance by Sm-modulated redox of $MnCeSmTiO_x$ mesoporous amorphous oxides for low-temperature NH_3-SCR of NO, ACS Catal. 10 (16) (2020) 9034–9045.
[39] Y. Zheng, S. Thampy, N. Ashburn, S. Dillon, L. Wang, Y. Jangjou, K. Tan, F. Kong, Y. Nie, M.J. Kim, W.S. Epling, Y.J. Chabal, J.W.P. Hsu, K. Cho, Stable and active oxidation catalysis by cooperative lattice oxygen redox on $SmMn_2O_5$ mullite surface, J. Am. Chem. Soc. 141 (27) (2019) 10722–10728.
[40] D. Meng, W. Zhan, Y. Guo, Y. Guo, L. Wang, G. Lu, A highly effective catalyst of Sm-MnO_x for the NH_3-SCR of NO_x at low temperature: promotional role of Sm and its catalytic performance, ACS Catal. 5 (2015) 5973–5983.
[41] Y. Xin, H. Li, N. Zhang, Q. Li, Z. Zhang, X. Cao, P. Hu, L. Zheng, J.A. Anderson, Molecular-level insight into selective catalytic reduction of NO_x with NH_3 to N_2 over a highly efficient bifunctional V_a-MnO_x catalyst at low temperature, ACS Catal. 8 (6) (2018) 4937–4949.